Orbital Description of Landau Levels

Huan Wang,[1,2] Rui Shi,[1,2] Zhaochen Liu,[1,2] and Jing Wang[1,2,3,4,*]

[1]*State Key Laboratory of Surface Physics and Department of Physics, Fudan University, Shanghai 200433, China*
[2]*Shanghai Research Center for Quantum Sciences, Shanghai 201315, China*
[3]*Institute for Nanoelectronic Devices and Quantum Computing, Fudan University, Shanghai 200433, China*
[4]*Hefei National Laboratory, Hefei 230088, China*

We construct a minimal lattice model to provide an orbital description of lowest and first Landau levels. With the maximally localized Wannier functions with s, p_-, p_+ orbital characteristics, a three-orbital model is developed, where the lowest two Chern bands are flat with $\mathcal{C} = 1$. This model can be viewed as consecutive band inversions between these Wannier states at Γ and K in momentum space, which adiabatically connects the atomic insulator limit to Landau level physics. Interestingly, many-body exact diagonalization and entanglement spectrum analysis suggest that the Abelian states can appear in the 1/3-filled lowest Chern band, while the signatures of the non-Abelian states are found in the half-filled first Chern band. This construction can be further extended to realize flat Chern bands resembling the higher Landau levels. Our results offer a new perspective to understand the lattice analogue of Landau levels, potentially enabling the realization of the fascinating topological phenomena at higher temperatures.

Introduction.— The recent discovery of the Abelian fractional Chern insulators (FCI) at zero magnetic field, dubbed fractional quantum anomalous Hall state in moiré $MoTe_2$ and pentalayer graphene [1–5] has generated intense interest in this new state of matter [6–19]. The emergence of the fractional topological states is attributed to the existence of flat Chern bands [20–25] with nearly ideal quantum geometry in moiré superlattice, which resembles the lowest Landau level (LLL). The exotic non-Abelian topological orders [26], such as Moore-Read states [27–30] or Read-Rezayi state [31] are predicted to exist in the partially filled first Landau level (1LL). These states support non-Abelian quasiparticle excitations [28] and could be utilized as a platform for fault-tolerant quantum computation [32, 33]. This raises an interesting question [34–39]: Is it possible and how to construct a flat Chern band on the lattice which resembles the 1LL physics with non-Abelian statistics? A positive answer to this question could offer opportunity to realize non-Abelian fractionalization at elevated temperatures without magnetic field.

Here we construct a minimal lattice model with maximally localized Wannier functions (MLWFs) with s, p_-, p_+ orbital characteristics. The lowest two bands are flat with Chern number equal to 1, where they have band inversion at Γ, while the second lowest and highest bands invert at K. Interestingly, many-body exact diagonalization calculations are carried out with the Wannier functions, which suggests that 1/3-filled lowest Chern band (LCB) supports the Abelian states, while half-filled first Chern band (1CB) supports the non-Abelian states. The quantum geometry of the combined lowest two Chern bands is close to the ideal value of the combined lowest two LLs. Thus, the lowest two Chern bands constitute the lattice analogue of the LLL and 1LL. Our method can be further extended to realize flat Chern bands resembling the higher LLs, as well as cold atom systems.

Intuition.— As a starting point, to construct the Chern bands in lattice model, we should know the characteristics of the Wannier states. Previously, Qi constructed the one-dimensional MLWF in Chern bands that have a one-to-one mapping to the LLL wave functions in quantum Hall [23] of the form $\psi_{0,K_y}(x,y) \sim e^{iK_y y} H_0(x') e^{-x'^2/2l_B^2}$, where $x' \equiv x - K_y \ell_B^2$. $H_0\left(x - K_y \ell_B^2\right)$ is the Hermite polynomial for $n = 0$ LLL, and $H_0(x') e^{-x'^2/2l_B^2} = e^{-x'^2/2l_B^2}$ is related to MLWF of Chern band and is s orbital like in one dimension. Intuitively, when the construction of more generic wave functions of Chern bands generalizes to 1LL, the MLWF of Chern bands maps to $H_1(x') e^{-x'^2/2l_B^2} = 2x' e^{-x'^2/2l_B^2}$, which resembles p orbital. Intuitively, at least the Wannier states with orbital characteristics s and p are needed to construct the Chern band that resembles 1LL physics.

Model and adiabatic connection.— We begin with a minimal continuum model in which itinerant electrons couple to a layer pseudospin skyrmion lattice. This model could well describe the consecutive topologically nontrivial flat bands in twisted homobilayer $MoTe_2$ around twist angle 2° [39–45],

$$\mathcal{H}_0 = \frac{\mathbf{p}^2}{2m} + \mathcal{J}\boldsymbol{\sigma} \cdot \mathbf{S}(\mathbf{r}). \tag{1}$$

Here $\boldsymbol{\sigma}$ is the pseudospin operator representing the degree of freedom of the layer, $\mathbf{S}(\mathbf{r}) = \mathbf{S}(\mathbf{r}+\mathbf{a}_{1,2})$ represents the periodic moiré potential and is naturally coupled to the pseudospin of the layer with strength $\mathcal{J}$. When the twist angle is small, the moiré potential dominates $\mathcal{J} \gg \hbar^2/ma^2$ and enforces local electron layer polarization align with $\mathbf{S}(\mathbf{r})$, which in turn induces a pseudospin Berry phase. This can be seen explicitly by a position-dependent $SU(2)$ unitary transformation $\mathbf{U}(\mathbf{r})$ that rotates the pseudo-spin texture $\mathbf{S}(\mathbf{r})$ into $S(\mathbf{r})\hat{z}$ and introduces a gauge field $\mathbf{A}_j = (i\hbar/e)\mathbf{U}^\dagger \partial_j \mathbf{U}$. For large $\mathcal{J}$, we can further project the Hamiltonian onto the low energy

manifold of local layer polarized electrons and obtain the effective Hamiltonian for the low energy band as

$$\mathcal{H}_{\text{eff}} = \frac{(\mathbf{p} - e\mathbf{A}(\mathbf{r}))^2}{2m} + \sum_{j=x,y} \frac{\hbar^2}{8m} (\partial_j \hat{\mathbf{S}})^2 - \mathcal{J} S(\mathbf{r}), \quad (2)$$

where $\mathbf{A}(\mathbf{r})$ is the $\downdownarrows$ component of the emergent $SU(2)$ gauge field, with $\nabla \times \mathbf{A}(\mathbf{r}) \equiv B^e(\mathbf{r}) = (\hbar/2e)\hat{\mathbf{S}} \cdot (\partial_x \hat{\mathbf{S}} \times \partial_y \hat{\mathbf{S}})$ be spatially non-uniform. $\mathcal{H}_{\text{eff}}$ describes a pseudospinless electron in a magnetic field when the last term in Eq. (2) is a constant, where the energy bands form dispersive LL. However, the potential $\mathbf{S}(\mathbf{r})$ fluctuates (sometimes wildly) according to the different local layer structures in the moiré system, so $S(\mathbf{r})$ is no longer generically constant. For large $\mathcal{J}$, the last term in Eq. (2) may dominate and its minimum forms a potential trap. Each trap has the form as $-JS(\mathbf{r}) \sim (\mathbf{r} - \mathbf{r}_{\min})^2 + O(\mathbf{r} - \mathbf{r}_{\min})^3$, which respects the rotational symmetry around the minimum, thus s, p, d type orbitals emerge in the low-energy bands [46–48]. Thus, in this limit, $\mathcal{H}_{\text{eff}}$ describes the orbital hopping with effective magnetic flux.

From such observations, we see that $\mathcal{H}_{\text{eff}}$ actually links effective atomic orbital and LL physics in the low energy manifold. This is made clearly by calculating the band structure of $\mathcal{H}_0$ when we take $\mathbf{S}(\mathbf{r}) = \mathbf{N}(\mathbf{r})/N^{\lambda}(\mathbf{r})$ with

$$\mathbf{N}(\mathbf{r}) = \frac{1}{\sqrt{2}} \sum_{j=1}^{6} e^{i\mathbf{q}_j \cdot \mathbf{r}} \hat{\mathbf{e}}_j + N_0 \hat{z}, \quad (3)$$

where $\hat{\mathbf{e}}_j = (i\alpha \sin\theta_j, -i\alpha \cos\theta_j, -1)/\sqrt{2}$, $\mathbf{q}_j = (4\pi/\sqrt{3}a)(\cos\theta_j, \sin\theta_j)$, and the angles satisfy $\theta_2 = \theta_1 + 2\pi/3$, $\theta_3 = \theta_1 + 4\pi/3$, and $\theta_{j+3} = \theta_j + \pi$. This pseudospin texture can be viewed as a sum of three pseudospin spirals forming a triangular skyrmion lattice [49–52], and the normalization is controlled by λ. When $\lambda = 1$, $S(\mathbf{r})$ becomes spatially uniform, and the low energy bands of $\mathcal{H}_0$ are flat Chern bands with $\mathcal{C} = 1$, as shown in Fig. 1(e). The lowest two Chern bands are dispersive LL, where their wave functions overlap with the corresponding flat LL exceed 99% [53]. For simplicity, we label them as LLL and 1LL, respectively. Conversely, when $\lambda \to 0$, the minimum of $-JS(\mathbf{r})$ forms a moiré triangular lattice (see Fig. 1(g)), and three lowest bands in Fig. 1(a) are topologically trivial flat bands resembling the atomic insulator limit, which emerge from s, p_-, p_+ orbital hopping on a triangular lattice.

Fig. 1 display the evolution of the band structures from flat topologically trivial bands to flat Chern bands. As λ changes from 0 to 1, the lowest three bands invert while their s, p_-, p_+ orbital characteristics remain. To see the band inversion clearly, we graphically depict the overlap of the Bloch states with trial Wannier functions of s, p_-, and p_+ orbitals, symbolized by blue, green, and red, respectively. The lowest three bands first invert with the upper band at M and their Chern numbers become $\mathcal{C} = [0, 0, 3]$ as shown in Fig. 1(b), then the second and third

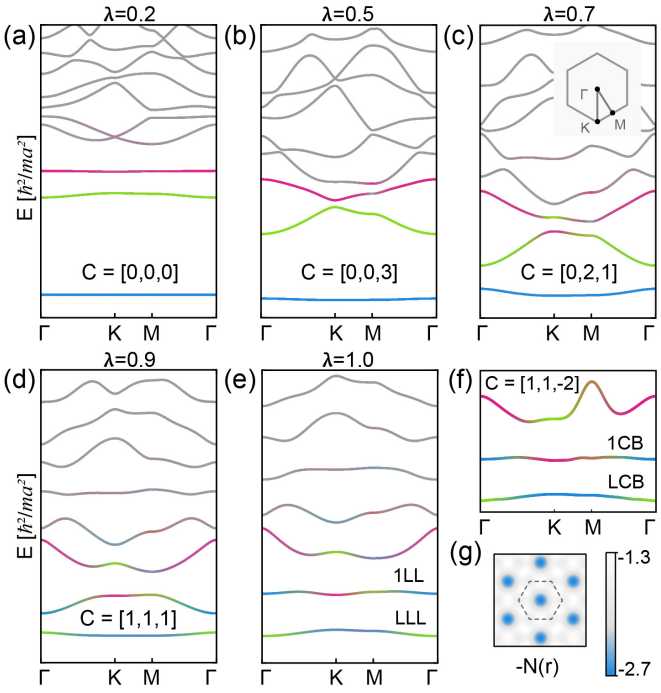

FIG. 1. Band structures and adiabatic connection from atomic insulator to LL. (a)-(e) The lowest few bands of $\mathcal{H}_0$ with different normalization parameter λ, where the overlap between Bloch state and Wannier function is labeled as different colors, and $\mathcal{C}$ denotes the Chern number of lowest three bands. The inset in (c) shows the Brillouin zone (BZ). (f) Band structure of the minimal three-orbital tight-binding model. (g) Real space distribution of $-N(\mathbf{r})$. The parameters are $J/(\hbar^2/ma^2) = 52\pi^2$, $\alpha = 1$ and $N_0 = 0.28$.

lowest bands invert at K and switch Chern numbers to $\mathcal{C} = [0, 2, 1]$ as in Fig. 1(c), finally the lowest and second lowest bands invert at Γ and Chern numbers becomes $\mathcal{C} = [1, 1, 1]$ as in Fig. 1(d,e). The lowest three Chern bands are isolated in Fig. 1(e). The orbital characteristics of the LLL and 1LL here are consistent with the mapping from the hybrid Wannier functions of Chern band to LL wave functions in quantum Hall [23].

Wannier projection.— Now we demonstrate that s, p_-, p_+ orbitals constitute a complete subspace to describe LLL and 1LL. By constructing the MLWFs [54–57] from the continuum model, a three-orbital model is developed to describe the lowest two Chern bands in Fig. 1(e), with the Wannier orbitals forming a triangular lattice. The minimal model includes hopping up to the fifteenth nearest neighbors, where its explicit form is in Supplemental Materials [53]. The band structure in Fig. 1(e) does not possess a local gap below which the total Chern number is zero. A set of frozen states is chosen to preserve the topology of the focused Chern bands and the band disentanglement [58] process is then performed to avoid the Wannier obstruction [59]. We choose the lowest two Chern bands as frozen states, and get the minimal tight-

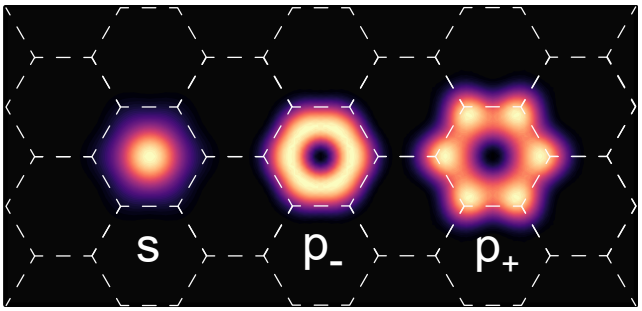

FIG. 2. The MLWFs of the lowest few bands in Fig. 1(e) with s, p_-, p_+ orbital characteristics, and the while hexagon labels Wigner-Seitz cell.

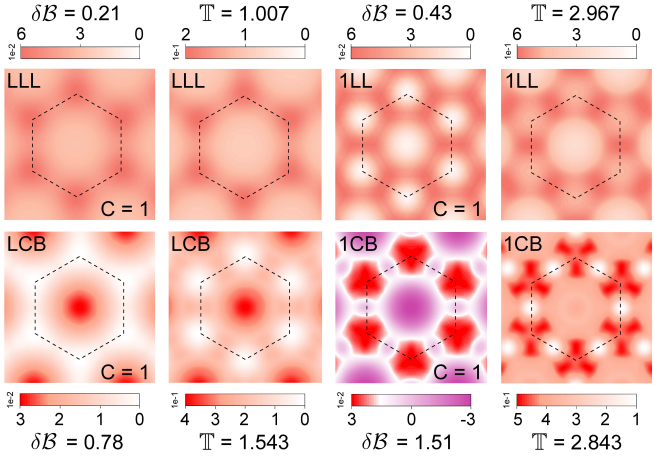

FIG. 3. The distribution of Berry curvature $\mathcal{B}(\mathbf{k})$ and trace of Fubini-Study metric $\mathrm{Tr}[g(\mathbf{k})]$ for the lowest two bands of continuum model and tight-binding model in the BZ. BZ is labelled by dashed hexagon. The fluctuation of Berry curvature $\delta\mathcal{B}$ are relatively larger in Chern bands compared LL, and thus $\mathbb{T}$ deviate more in Chern bands from the ideal LL.

binding model where only MLWFs with s, p_-, p_+ orbitals characteristics are included. The corresponding band structure is calculated in Fig. 1(f). The MLWFs of s, p_-, p_+ orbitals are shown in Fig. 2. The lowest two bands projected from the LLL and 1LL are well reconstructed in Fig. 1(f), which are labeled the LCB and 1CB, respectively.

Two band geometry indicators are employed to evaluate the different between Chern bands and LL [60–67], namely Berry curvature fluctuation $\delta\mathcal{B}$ and average trace condition $\mathbb{T}$ (non-negative) defined as

$$(\delta\mathcal{B})^2 \equiv \frac{\Omega_{\mathrm{BZ}}}{4\pi^2}\int_{\mathrm{BZ}} d\mathbf{k}\left(\mathcal{B}(\mathbf{k}) - \frac{2\pi\mathcal{C}}{\Omega_{\mathrm{BZ}}}\right)^2, \tag{4}$$

$$\mathbb{T} \equiv \int_{\mathrm{BZ}} d\mathbf{k}\left[\mathrm{Tr}(g(\mathbf{k}))\right], \tag{5}$$

where $\mathcal{B}(\mathbf{k}) \equiv -2\mathrm{Im}(\eta^{xy})$ is the Berry curvature, $g(\mathbf{k}) \equiv \mathrm{Re}(\eta^{\mu\nu})$ is the Fubini-Study metric, and $\eta^{\mu\nu}(\mathbf{k}) \equiv \langle\partial^\mu u_{\mathbf{k}}|\left(1-|u_{\mathbf{k}}\rangle\langle u_{\mathbf{k}}|\right)|\partial^\nu u_{\mathbf{k}}\rangle$ is the quantum geometric tensor, $\mathcal{C} \equiv (1/2\pi)\int d^2\mathbf{k}\mathcal{B}(\mathbf{k})$, Ω_{BZ} is area of BZ. We plot the distribution of $\mathcal{B}(\mathbf{k})$ and $\mathrm{Tr}[g(\mathbf{k})]$ of the BZ in Fig. 3. For LLL and 1LL, $\mathcal{B}(\mathbf{k})$ remain positive throughout the whole BZ and the distribution is quite homogenous with relatively small fluctuation $\delta\mathcal{B}$, and $\mathbb{T}$ is almost ideal ($\mathbb{T} = 2n+1$ for nth flat LL). However, in the tight-binding model, $\mathcal{B}(\mathbf{k})$ is no longer homogenous but concentrates around the band inversion points, and their sign is not always positive (such as in 1CB) throughout the BZ, leading to relatively large fluctuation $\delta\mathcal{B}$ and deviation of $\mathbb{T}$ from the ideal value in LL.

These differences between Chern bands of the tight-binding model and dispersive LL of the continuum model are inevitable, since we project out the higher energy degree of freedom in the continuum model and keep only s, p_-, p_+ Wannier states. Then the band inversion among them naturally lead to Berry curvature concentration. Especially for the 1CB, the band inversion between p_- and s contribute the negative $\mathcal{B}(\mathbf{k})$ around Γ point and the inversion between p_- and p_+ contribute the positive $\mathcal{B}(\mathbf{k})$ around K and K' points. Remarkably, we will see that a non-Abelian state can occur even when the Berry curvature fluctuates strongly.

Exact diagonalization.— To explore whether the non-Abelian state can appear in 1CB, we now study many-body physics at fractional filling in these Chern bands via numerical diagonalization. To make the many-body calculation tractable, we restrict our variational Hilbert space to that in which N_{uc} electrons fill the LCB and $N_e - N_{\mathrm{uc}}$ electrons remain in the 1CB where N_e is the number of electrons. The electron-electron interaction Hamiltonian is obtained by projecting the realistic Coulomb interaction into the MLWFs and keeping the leading terms [53], which is defined as

$$\mathcal{H}_{\mathrm{int}} = \frac{U}{2}\sum_{i,a\neq b} n_{i,a}n_{i,b} + V\sum_{\langle ij\rangle,a,b} n_{i,a}n_{j,b}, \tag{6}$$

where $a,b = (s,\ p_-,\ p_+)$, $\langle ij\rangle$ means nearest-neighbor, U and V are the strength of onsite and nearest-neighbor interaction which is independent of orbital degree of freedom. We ignore the kinetic energy since these two lowest Chern bands are quite flat.

Fig. 4(a) display the many-body spectra at filling $\nu = 1/3$ (namely, 1/3 filling of LCB) as a function of crystal momentum $\mathbf{k} = k_1\mathbf{T}_1 + k_1\mathbf{T}_2$, which is labeled as $k = k_1 + N_1k_2$. Here $k_i = 0, ..., N_i - 1$ $(i = 1, 2)$ for system size $N_{\mathrm{uc}} = N_1 \times N_2$ with filled particle number $N_e = \nu N_{\mathrm{uc}}$ and $\mathbf{T}_i$ are basis vectors of crystal momentum. The cluster size is chosen as $N_{\mathrm{uc}} = 4\times 6$, and $U = 1$ and $V = 0$. There are 3 nearly degenerate ground states well separated by a sizable energy gap from excited states. The approximate ground state degeneracy matches with the expected topological degeneracy of a

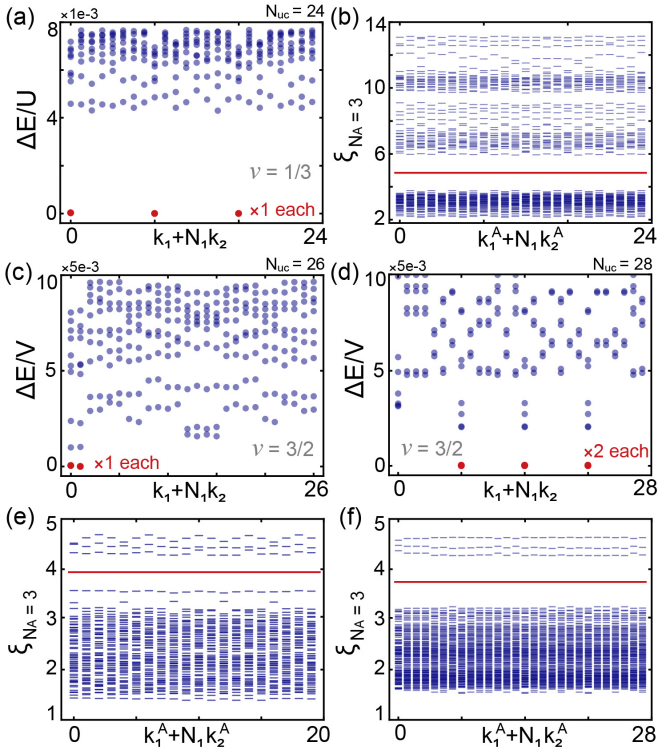

FIG. 4. Exact diagonalization and PES for fractional filled CB. (a) Low energy many-body energy spectrum for 1/3 filled LCB with $N_{\rm uc} = 24$. (b) PES with $N_A = 3$ for the three degenerate ground states in (a), where $\rho = (1/d)\sum_i^d |\Psi_i\rangle\langle\Psi_i|$. d is the degeneracy of ground states. (c), (d) Energy spectrum for 1/2 filled 1CB with $N_{\rm uc} = 26$ and $N_{\rm uc} = 28$. (e), (f) PES with $N_A = 3$ for the six degenerate ground states in $N_{\rm uc} = 20$ and $N_{\rm uc} = 28$. Here we only show the lowest energy per momentum sectors in addition to the degenerate ground state.

fractional QH state on a torus. We further calculated different cluster sizes with all other parameters fixed and find the gap remains indicating its existence in the thermodynamic limit [53]. The lattice momenta of the degenerate ground states have linear indices $(0, 8, 16)$ and are in precise agreement with the generalized Pauli principle, which is the hallmark of FCI at 1/3 filling [25]. To further confirm and distinguish FCI and other competing phases, we subsequently calculated the particle entanglement spectrum (PES) which encodes the information of the quasihole excitations [68, 69], by dividing the whole system into $N_A = 3$ and $N_e - N_A$ particles. As shown in Fig. 4(b), we find that there is a clear entanglement gap separating the low-lying PES levels from higher ones for degenerate many body ground states. The number of PES levels below the gap exactly matches the typical counting of quasiparticle excitations resulting from the generalized Pauli principle of 1/3 Laughlin state. These numerical results suggest that LCB resembles LLL.

Fig. 4(c,d) show the many-body spectra at filling $\nu = 3/2$ (that is, 1/2 filling of 1CB assuming full spin polarization). The exact diagonalization is performed on finite-size torus with $U = 1.3$ and $V = 1$. For $N_{\rm uc} = 2\times 13$, the number of electrons occupying the 1CB is odd (13), while for $N_{\rm uc} = 2 \times 14$, it is even (14). In these two cases, we observe two-fold and sixfold ground state quasi-degeneracies in Fig. 4(c) and 4(d), respectively. These are precisely the degeneracies expected for a Moore-Read state on the torus due to an even-odd effect [28, 70, 71], and the enhancement of gap indicates its existence in the thermodynamic limit. The lattice momenta at which these ground states occur also match the momenta of non-Abelian $\nu = 1/2$ FCI based on the fractional quantum Hall-FCI folding scheme [25, 72]. We also calculate spectrum under the twist boundary condition to check the finite-size effect [53], where the momentum of single particle shifts to $k_i \to k_i + (\theta_i/2\pi)\mathbf{T}_i$ providing an effective way to scan all momenta in the BZ near continuously. We find the quasi-degenerate ground states remain well separated from the other low-energy excitation spectrum, indicating the robustness of the excitation gap [53].

To exclude other competing phases in the half-filled 1CB, we further calculate PES with $N_A = 3$ for $N_{\rm uc} = 4 \times 5$ and $N_{\rm uc} = 2 \times 14$ in Fig. 4(e,f), respectively. A clear entanglement gap separating the low-lying PES levels from higher ones is identified. The number of PES levels below this gap exactly matches the typical counting of quasiparticle excitations resulting from the generalized Pauli principle of the non-Abelian Pfaffian or anti-Pfaffian state [25] (at most 2 particles in 4 consecutive orbitals). The particle-hole symmetry is explicitly broken by the non-uniform quantum geometries here, thus the particle-hole Pfaffian state [73] is less likely to be a competing phase compared to Pfaffian and anti-Pfaffian states [74]. The concrete nature of the non-Abelian state need more detailed examination by wave function overlap. From the correspondence between the PES and the quasiparticle excitations, the numerical results further suggest the non-Abelian nature of this half-filled state.

Discussions.— The method studied here can be further generalized to Chern bands with band inversion resembling higher LL. Concretely, an ideal local band inversion is introduced with a simple $\mathbf{k}\cdot\mathbf{p}$ model [75]

$$\mathcal{H}_{\rm local}(\mathbf{k}) = \begin{pmatrix} \alpha\mathbf{k}^2 + \Delta & v_F k_+ \\ v_F k_- & -\beta\mathbf{k}^2 - \Delta \end{pmatrix}, \qquad (7)$$

where $k_\pm = k_x \pm ik_y$. When $\Delta = -v_F^2/2(\alpha+\beta)$, both bands satisfy the trace and determinant conditions at any $\mathbf{k}$ with $g_{\mu\nu}(\mathbf{k}) = (1/2)\,|\mathcal{B}(\mathbf{k})|\,\delta_{\mu\nu}$. Such an ideal local band inversion always lead to local Chern number $\mathcal{C}_{\rm local} = 1$ and local average trace condition $\mathbb{T}_{\rm local} = 1$ when the integration is applied around the band inversion point. This well explains that the orbitals s, p_-, p_+ constitute a complete subspace to describe the LLL and 1LL shown in Fig. 1 and Fig. 3. For the LCB, there is only an inversion of the band between s and p_- at Γ,

thus $\mathcal{B}(\mathbf{k})$ and $\mathrm{Tr}[g(\mathbf{k})]$ concentrate around Γ, and the integral of them around Γ gives the Chern number of the band $\mathcal{C} = 1$ and $\mathbb{T} \approx 1$. For the 1CB, there are p_- and s band inversion at Γ, as well as p_- and p_+ band inversion at K, the integral of $\mathcal{B}(\mathbf{k})$ around Γ and K is -1 and $+1$, respectively, while local $\mathbb{T}$ around Γ and K are both nearly 1, then the sum of them finally leads to the band Chern number $\mathcal{C} = 2 - 1 = 1$ and $\mathbb{T} = |2| + |-1| = 3$. Such processes could be applied to higher Chern bands. As shown in Fig. 1(b,e), the band inversion happened at M between p_+ and higher d orbital provide local Chern number $\mathcal{C}_{\mathrm{local}} = 1$ and local $\mathbb{T}_{\mathrm{local}} = 1$ at each M, combined with the p_+ and p_- band inversion at K, we get Chern number $\mathcal{C} = 3 - 2 = 1$ and $\mathbb{T} = |3| + |-2| = 5$ for second Chern bands (namely, the third band counting from below), which is the ideal number for second LL. The quantum geometry of these constructed Chern bands matches with that of the generalized LL [76]. It is worth mentioning that the Chern bands from such construction only have perfect quantum weight at the cost of Berry curvature flatness, since $\mathcal{B}(\mathbf{k})$ always concentrates at the local band inversion point. To obtain the FCI state in the partially filled Chern bands, a delicate balance between $\mathcal{B}(\mathbf{k})$ flatness and ideal $\mathbb{T}$ should be considered. The construction of the projected Hamiltonian within the triangular lattice here can be directly generalized to the square lattice, provided that $\mathbf{S}(\mathbf{r})$ exhibits C_4 symmetry. Furthermore, our results could be applied to cold atom systems [77], since only short-range density-density interactions are required.

We point out that the orbital construction of LL here is consistent with the higher vortexability for 1LL proposed in Ref. [34]. The 1CB here is not self-vortexable because of its large value of $\mathbb{T}$. When we combine LCB and 1CB together, we can see a nearly ideal $\mathbb{T} = 2.2$ for the lowest two Chern bands, since they originate from band inversion between p_- and p_+ at K point.

Acknowledgment. We thank Biao Lian and Dung-Hai Lee for helpful discussions. This work is supported by the Natural Science Foundation of China through Grants No. 12350404 and No. 12174066, the Innovation Program for Quantum Science and Technology through Grant No. 2021ZD0302600, the Science and Technology Commission of Shanghai Municipality under Grants No. 23JC1400600 and No. 2019SHZDZX01. H.W. and R.S. contributed equally to this work.

* wjingphys@fudan.edu.cn

[1] J. Cai, E. Anderson, C. Wang, X. Zhang, X. Liu, W. Holtzmann, Y. Zhang, F. Fan, T. Taniguchi, K. Watanabe, Y. Ran, T. Cao, L. Fu, D. Xiao, W. Yao, and X. Xu, Signatures of fractional quantum anomalous hall states in twisted mote2, Nature **622** (2023).

[2] Y. Zeng, Z. Xia, K. Kang, J. Zhu, P. Knüppel, C. Vaswani, K. Watanabe, T. Taniguchi, K. F. Mak, and J. Shan, Thermodynamic evidence of fractional chern insulator in moiré mote2, Nature **622**, 69 (2023).

[3] H. Park, J. Cai, E. Anderson, Y. Zhang, J. Zhu, X. Liu, C. Wang, W. Holtzmann, C. Hu, Z. Liu, T. Taniguchi, K. Watanabe, J.-H. Chu, T. Cao, L. Fu, W. Yao, C.-Z. Chang, D. Cobden, D. Xiao, and X. Xu, Observation of fractionally quantized anomalous hall effect, Nature **622** (2023).

[4] F. Xu, Z. Sun, T. Jia, C. Liu, C. Xu, C. Li, Y. Gu, K. Watanabe, T. Taniguchi, B. Tong, J. Jia, Z. Shi, S. Jiang, Y. Zhang, X. Liu, and T. Li, Observation of integer and fractional quantum anomalous hall effects in twisted bilayer mote_2, Phys. Rev. X **13**, 031037 (2023).

[5] Z. Lu, T. Han, Y. Yao, A. P. Reddy, J. Yang, J. Seo, K. Watanabe, T. Taniguchi, L. Fu, and L. Ju, Fractional quantum anomalous hall effect in multilayer graphene, Nature **626**, 759 (2024).

[6] H. Li, U. Kumar, K. Sun, and S.-Z. Lin, Spontaneous fractional chern insulators in transition metal dichalcogenide moiré superlattices, Phys. Rev. Res. **3**, L032070 (2021).

[7] V. Crépel and L. Fu, Anomalous hall metal and fractional chern insulator in twisted transition metal dichalcogenides, Phys. Rev. B **107**, L201109 (2023).

[8] N. Morales-Durán, J. Wang, G. R. Schleder, M. Angeli, Z. Zhu, E. Kaxiras, C. Repellin, and J. Cano, Pressure-enhanced fractional chern insulators along a magic line in moiré transition metal dichalcogenides, Phys. Rev. Res. **5**, L032022 (2023).

[9] J. Yu, J. Herzog-Arbeitman, M. Wang, O. Vafek, B. A. Bernevig, and N. Regnault, Fractional chern insulators versus nonmagnetic states in twisted bilayer mote_2, Phys. Rev. B **109**, 045147 (2024).

[10] J. Dong, J. Wang, P. J. Ledwith, A. Vishwanath, and D. E. Parker, Composite fermi liquid at zero magnetic field in twisted mote_2, Phys. Rev. Lett. **131**, 136502 (2023).

[11] H. Goldman, A. P. Reddy, N. Paul, and L. Fu, Zero-field composite fermi liquid in twisted semiconductor bilayers, Phys. Rev. Lett. **131**, 136501 (2023).

[12] C. Wang, X.-W. Zhang, X. Liu, Y. He, X. Xu, Y. Ran, T. Cao, and D. Xiao, Fractional chern insulator in twisted bilayer mote_2, Phys. Rev. Lett. **132**, 036501 (2024).

[13] Y. Jia, J. Yu, J. Liu, J. Herzog-Arbeitman, Z. Qi, H. Pi, N. Regnault, H. Weng, B. A. Bernevig, and Q. Wu, Moiré fractional chern insulators. i. first-principles calculations and continuum models of twisted bilayer mote_2, Phys. Rev. B **109**, 205121 (2024).

[14] N. Morales-Durán, N. Wei, J. Shi, and A. H. MacDonald, Magic angles and fractional chern insulators in twisted homobilayer transition metal dichalcogenides, Phys. Rev. Lett. **132**, 096602 (2024).

[15] Z. Ji, H. Park, M. E. Barber, C. Hu, K. Watanabe, T. Taniguchi, J.-H. Chu, X. Xu, and Z. xun Shen, Local probe of bulk and edge states in a fractional chern insulator (2024), arXiv:2404.07157 [cond-mat.str-el].

[16] E. Redekop, C. Zhang, H. Park, J. Cai, E. Anderson, O. Sheekey, T. Arp, G. Babikyan, S. Salters, K. Watanabe, T. Taniguchi, X. Xu, and A. F. Young, Direct magnetic imaging of fractional chern insulators in twisted mote_2 with a superconducting sensor (2024), arXiv:2405.10269 [cond-mat.mes-hall].

[17] K. Kang, B. Shen, Y. Qiu, Y. Zeng, Z. Xia, K. Watan-

abe, T. Taniguchi, J. Shan, and K. F. Mak, Evidence of the fractional quantum spin hall effect in moiré mote2, Nature **628**, 522 (2024).
[18] J. Xie, Z. Huo, X. Lu, Z. Feng, Z. Zhang, W. Wang, Q. Yang, K. Watanabe, T. Taniguchi, K. Liu, Z. Song, X. C. Xie, J. Liu, and X. Lu, Even- and odd-denominator fractional quantum anomalous hall effect in graphene moire superlattices (2024), arXiv:2405.16944 [cond-mat.mes-hall].
[19] Z. Lu, T. Han, Y. Yao, J. Yang, J. Seo, L. Shi, S. Ye, K. Watanabe, T. Taniguchi, and L. Ju, Extended quantum anomalous hall states in graphene/hbn moiré superlattices (2024), arXiv:2408.10203 [cond-mat.mes-hall].
[20] E. Tang, J.-W. Mei, and X.-G. Wen, High-temperature fractional quantum hall states, Phys. Rev. Lett. **106**, 236802 (2011).
[21] K. Sun, Z. Gu, H. Katsura, and S. Das Sarma, Nearly flatbands with nontrivial topology, Phys. Rev. Lett. **106**, 236803 (2011).
[22] T. Neupert, L. Santos, C. Chamon, and C. Mudry, Fractional quantum hall states at zero magnetic field, Phys. Rev. Lett. **106**, 236804 (2011).
[23] X.-L. Qi, Generic wave-function description of fractional quantum anomalous hall states and fractional topological insulators, Phys. Rev. Lett. **107**, 126803 (2011).
[24] D. Sheng, Z.-C. Gu, K. Sun, and L. Sheng, Fractional quantum hall effect in the absence of landau levels, Nature Commun. **2**, 389 (2011).
[25] N. Regnault and B. A. Bernevig, Fractional chern insulator, Phys. Rev. X **1**, 021014 (2011).
[26] R. Willett, J. P. Eisenstein, H. L. Störmer, D. C. Tsui, A. C. Gossard, and J. H. English, Observation of an even-denominator quantum number in the fractional quantum hall effect, Phys. Rev. Lett. **59**, 1776 (1987).
[27] G. Moore and N. Read, Nonabelions in the fractional quantum hall effect, Nucl. Phys. B **360**, 362 (1991).
[28] N. Read and D. Green, Paired states of fermions in two dimensions with breaking of parity and time-reversal symmetries and the fractional quantum hall effect, Phys. Rev. B **61**, 10267 (2000).
[29] P. Bonderson, A. Kitaev, and K. Shtengel, Detecting non-abelian statistics in the $\nu = 5/2$ fractional quantum hall state, Phys. Rev. Lett. **96**, 016803 (2006).
[30] M. Levin, B. I. Halperin, and B. Rosenow, Particle-hole symmetry and the pfaffian state, Phys. Rev. Lett. **99**, 236806 (2007).
[31] N. Read and E. Rezayi, Beyond paired quantum hall states: Parafermions and incompressible states in the first excited landau level, Phys. Rev. B **59**, 8084 (1999).
[32] A. Y. Kitaev, Fault-tolerant quantum computation by anyons, Ann. Phys. **303**, 2 (2003).
[33] C. Nayak, S. H. Simon, A. Stern, M. Freedman, and S. Das Sarma, Non-abelian anyons and topological quantum computation, Rev. Mod. Phys. **80**, 1083 (2008).
[34] M. Fujimoto, D. E. Parker, J. Dong, E. Khalaf, A. Vishwanath, and P. Ledwith, Higher vortexability: zero field realization of higher landau levels (2024), arXiv:2403.00856 [cond-mat.mes-hall].
[35] A. P. Reddy, N. Paul, A. Abouelkomsan, and L. Fu, Non-abelian fractionalization in topological minibands, Phys. Rev. Lett. **133**, 166503 (2024).
[36] C. Xu, N. Mao, T. Zeng, and Y. Zhang, Multiple chern bands in twisted $mote_2$ and possible non-abelian states (2024), arXiv:2403.17003 [cond-mat.str-el].
[37] C.-E. Ahn, W. Lee, K. Yananose, Y. Kim, and G. Y. Cho, Non-abelian fractional quantum anomalous hall states and first landau level physics in second moiré band of twisted bilayer mote2 (2024), arXiv:2403.19155 [cond-mat.str-el].
[38] F. Chen, W.-W. Luo, W. Zhu, and D. N. Sheng, Robust non-abelian even-denominator fractional chern insulator in twisted bilayer $mote_2$ (2024), arXiv:2405.08386 [cond-mat.str-el].
[39] C. Wang, X.-W. Zhang, X. Liu, J. Wang, T. Cao, and D. Xiao, Higher landau-level analogues and signatures of non-abelian states in twisted bilayer $mote_2$ (2024), arXiv:2404.05697 [cond-mat.str-el].
[40] F. Wu, T. Lovorn, E. Tutuc, I. Martin, and A. H. MacDonald, Topological insulators in twisted transition metal dichalcogenide homobilayers, Phys. Rev. Lett. **122**, 086402 (2019).
[41] T. Devakul, V. Crépel, Y. Zhang, and L. Fu, Magic in twisted transition metal dichalcogenide bilayers, Nature Commun. **12**, 6730 (2021).
[42] A. P. Reddy, F. Alsallom, Y. Zhang, T. Devakul, and L. Fu, Fractional quantum anomalous hall states in twisted bilayer $mote_2$ and wse_2, Phys. Rev. B **108**, 085117 (2023).
[43] X.-W. Zhang, C. Wang, X. Liu, Y. Fan, T. Cao, and D. Xiao, Polarization-driven band topology evolution in twisted mote2 and wse2, Nature Commun. **15**, 4223 (2024).
[44] B. Li and F. Wu, Variational mapping of chern bands to landau levels: Application to fractional chern insulators in twisted $mote_2$ (2024), arXiv:2405.20307 [cond-mat.mes-hall].
[45] J. Shi, N. Morales-Durán, E. Khalaf, and A. H. MacDonald, Adiabatic approximation and aharonov-casher bands in twisted homobilayer transition metal dichalcogenides, Phys. Rev. B **110**, 035130 (2024).
[46] T. Kariyado and A. Vishwanath, Flat band in twisted bilayer bravais lattices, Phys. Rev. Res. **1**, 033076 (2019).
[47] M. Angeli and A. H. MacDonald, γ valley transition metal dichalcogenide moiré bands, Proc. Natl. Acad. Sci. U.S.A. **118**, e2021826118 (2021).
[48] Z. Liu, H. Wang, and J. Wang, Magnetic moiré surface states and flat chern bands in topological insulators, Phys. Rev. B **106**, 035114 (2022).
[49] A. Tonomura, X. Yu, K. Yanagisawa, T. Matsuda, Y. Onose, N. Kanazawa, H. S. Park, and Y. Tokura, Real-space observation of skyrmion lattice in helimagnet mnsi thin samples, Nano Lett. **12**, 1673 (2012).
[50] K. Karube, J. S. White, D. Morikawa, M. Bartkowiak, A. Kikkawa, Y. Tokunaga, T. Arima, H. M. Rønnow, Y. Tokura, and Y. Taguchi, Skyrmion formation in a bulk chiral magnet at zero magnetic field and above room temperature, Phys. Rev. Mater. **1**, 074405 (2017).
[51] Y. Tokura and N. Kanazawa, Magnetic skyrmion materials, Chem. Rev. **121**, 2857 (2021).
[52] S.-Z. Lin and S. Hayami, Ginzburg-landau theory for skyrmions in inversion-symmetric magnets with competing interactions, Phys. Rev. B **93**, 064430 (2016).
[53] See supplemental material for technical details.
[54] G. Pizzi, V. Vitale, R. Arita, S. Blügel, F. Freimuth, G. Géranton, M. Gibertini, D. Gresch, C. Johnson, T. Koretsune, J. Ibañez-Azpiroz, H. Lee, J.-M. Lihm, D. Marchand, A. Marrazzo, Y. Mokrousov, J. I. Mustafa, Y. Nohara, Y. Nomura, L. Paulatto, S. Poncé, T. Pon-

weiser, J. Qiao, F. Thöle, S. S. Tsirkin, M. Wierzbowska, N. Marzari, D. Vanderbilt, I. Souza, A. A. Mostofi, and J. R. Yates, Wannier90 as a community code: new features and applications, J. Phys. Condens. Matter **32**, 165902 (2020).

[55] R. Sakuma, Symmetry-adapted wannier functions in the maximal localization procedure, Phys. Rev. B **87**, 235109 (2013).

[56] N. Marzari and D. Vanderbilt, Maximally localized generalized wannier functions for composite energy bands, Phys. Rev. B **56**, 12847 (1997).

[57] N. Marzari, A. A. Mostofi, J. R. Yates, I. Souza, and D. Vanderbilt, Maximally localized wannier functions: Theory and applications, Rev. Mod. Phys. **84**, 1419 (2012).

[58] I. Souza, N. Marzari, and D. Vanderbilt, Maximally localized wannier functions for entangled energy bands, Phys. Rev. B **65**, 035109 (2001).

[59] C. Brouder, G. Panati, M. Calandra, C. Mourougane, and N. Marzari, Exponential localization of wannier functions in insulators, Phys. Rev. Lett. **98**, 046402 (2007).

[60] S. A. Parameswaran, R. Roy, and S. L. Sondhi, Fractional chern insulators and the W_∞ algebra, Phys. Rev. B **85**, 241308 (2012).

[61] R. Roy, Band geometry of fractional topological insulators, Phys. Rev. B **90**, 165139 (2014).

[62] T. S. Jackson, R. Roy, and G. Möller, Geometric stability of topological lattice phases, Nature Commun. **6**, 8629 (2015).

[63] M. Claassen, C. H. Lee, R. Thomale, X.-L. Qi, and T. P. Devereaux, Position-momentum duality and fractional quantum hall effect in chern insulators, Phys. Rev. Lett. **114**, 236802 (2015).

[64] B. Mera and T. Ozawa, Kähler geometry and chern insulators: Relations between topology and the quantum metric, Phys. Rev. B **104**, 045104 (2021).

[65] T. Ozawa and B. Mera, Relations between topology and the quantum metric for chern insulators, Phys. Rev. B **104**, 045103 (2021).

[66] J. Wang, J. Cano, A. J. Millis, Z. Liu, and B. Yang, Exact landau level description of geometry and interaction in a flatband, Phys. Rev. Lett. **127**, 246403 (2021).

[67] P. J. Ledwith, A. Vishwanath, and D. E. Parker, Vortexability: A unifying criterion for ideal fractional chern insulators, Phys. Rev. B **108**, 205144 (2023).

[68] A. Sterdyniak, N. Regnault, and B. A. Bernevig, Extracting excitations from model state entanglement, Phys. Rev. Lett. **106**, 100405 (2011).

[69] A. Chandran, M. Hermanns, N. Regnault, and B. A. Bernevig, Bulk-edge correspondence in entanglement spectra, Phys. Rev. B **84**, 205136 (2011).

[70] M. Oshikawa, Y. B. Kim, K. Shtengel, C. Nayak, and S. Tewari, Topological degeneracy of non-abelian states for dummies, Ann. Phys. **322**, 1477 (2007).

[71] Z. Papić, F. D. M. Haldane, and E. H. Rezayi, Quantum phase transitions and the ν=5/2 fractional hall state in wide quantum wells, Phys. Rev. Lett. **109**, 266806 (2012).

[72] B. A. Bernevig and N. Regnault, Emergent many-body translational symmetries of abelian and non-abelian fractionally filled topological insulators, Phys. Rev. B **85**, 075128 (2012).

[73] D. T. Son, Is the composite fermion a dirac particle?, Phys. Rev. X **5**, 031027 (2015).

[74] E. H. Rezayi, Landau level mixing and the ground state of the $\nu = 5/2$ quantum hall effect, Phys. Rev. Lett. **119**, 026801 (2017).

[75] T. Tan and T. Devakul, Parent berry curvature and the ideal anomalous hall crystal, Phys. Rev. X **14**, 041040 (2024).

[76] Z. Liu, B. Mera, M. Fujimoto, T. Ozawa, and J. Wang, Theory of generalized landau levels and implication for non-abelian states (2024), arXiv:2405.14479 [cond-mat.mes-hall].

[77] J. Léonard, S. Kim, J. Kwan, P. Segura, F. Grusdt, C. Repellin, N. Goldman, and M. Greiner, Realization of a fractional quantum hall state with ultracold atoms, Nature **619**, 495 (2023).